

## Article

# Comparison of Stress Concentration Factors Obtained by Different Methods

Peter Sivák , Ingrid Delyová \*  and Jozef Bocko 

Department of Applied Mechanics and Mechanical Engineering, Faculty of Mechanical Engineering, Technical University of Košice, Letná 9, 042 00 Košice, Slovakia; peter.sivak@tuke.sk (P.S.); jozef.bocko@tuke.sk (J.B.)

\* Correspondence: ingrid.delyova@tuke.sk

**Abstract:** This paper offers a study regarding regression and correlation analysis and intercomparison of stress concentration factors obtained from FEM analysis with factors imported from external sources. The procedure for obtaining the stress concentration factors is implemented and demonstrated on the shape configuration of an axially symmetric structural element with offset, tension loading. It is a typical representation of stress concentrators of the shape-discontinuity-dimension-load configuration applied in structural elements mainly from the engineering and construction fields. The data thus obtained are then subjected to regression and simple correlation analysis. Three regression models based on 2nd- and 3rd-degree polynomials and power function are applied. These results are further subjected to a detailed procedure of comparison with the values of the stress concentration factors obtained from two other independent sources. Finally, a detailed analysis of the possible reasons for the registered value deviations is performed.

**Keywords:** stress concentrator; stress concentration factor; experimental and numerical stress analysis; regression analysis



**Citation:** Sivák, P.; Delyová, I.; Bocko, J. Comparison of Stress Concentration Factors Obtained by Different Methods. *Appl. Sci.* **2023**, *13*, 13328. <https://doi.org/10.3390/app132413328>

Academic Editors: Lubos Kascak and Emil Spišák

Received: 21 November 2023

Revised: 11 December 2023

Accepted: 14 December 2023

Published: 18 December 2023



**Copyright:** © 2023 by the authors. Licensee MDPI, Basel, Switzerland. This article is an open access article distributed under the terms and conditions of the Creative Commons Attribution (CC BY) license (<https://creativecommons.org/licenses/by/4.0/>).

## 1. Introduction

The determination of stress concentration factors and their subsequent implementation in the design process and condition assessment of structural elements and entire structures is an essential element in the prediction of the behavior of structures affected by the notch effect in different loading regimes. Historically, the problem of the notching effect was initially addressed analytically. However, it was limited to simple shape-discontinuity-dimension-load configurations and to the elastic deformation domain only. The present means of stress–strain analysis allow relatively efficient determination of the stress concentration factors analytically, experimentally and numerically, simultaneously in all their interaction possibilities of comparison and verification. Experimental methods with a significant degree of application include the planar and spatial transmission Photostress® method [1]. The obtained data of stress concentration factors are then arranged for the various shape-dimension-load configurations and the basic types of discontinuities of the structures, most often in the form of graphs, nomograms, or various approximation equations, dependencies, etc. Combined, experimental–analytical methods may also be applied. They are relatively faster and more efficient, although the results obtained are less accurate. However, nowadays, a number of new, specific and shape-complex structural elements are emerging for which such information is not available. In such cases, computer simulations and computer modelling are a suitable solution. They make it possible to subject a mathematical model of a real and shape-complex element to specific loads and thus to obtain information on the progress and distribution of stresses and, where appropriate, deformations. Such a model can then be subjected to optimization procedures and subsequently modified as required. An important element is the possibility of statistical and correlation evaluation of the obtained results. Of the available numerical methods, the finite element method is considered to be the most effective and the most widely used,

where, with the correct definition of boundary conditions and loads, the correct choice of the type and number of finite elements, etc., it is possible to obtain results comparable to experimental methods. These can then be applied for comparison and verification purposes as independent verification means in justified cases [2,3].

This paper does not seek to fundamentally question existing data, its sources and methods of acquisition, which have been with us, in some cases, for several decades. On the contrary, for a long period of time, they have been able to be applied relatively successfully in various fields of design and assessment of structural elements and entire structures, specifically from the fields of engineering and construction. However, if there is to be continuous progress and improvement in this field, it cannot only concern the relevant methods of construction and design but also the input data and, in particular, the means of obtaining them quickly, efficiently and economically. This also applies in full to the continuous improvement of the accuracy and relevance of these data. This paper, using the example of a simple and relatively frequently occurring shape-discontinuity-dimension-load configuration, should highlight the relevant state of the art and the associated problems.

## 2. Notches as Stress Concentrators

In practical applications of structural components, especially in the field of engineering and construction, it is often necessary to suddenly change the shape or cross-section of a component from a functional point of view. At the points of any cross-sectional and shape change in the structure (especially in cases of sudden changes), the continuity of the force flow is disturbed, the force lines are locally condensed, resulting in a local increase in the nominal stress. The presence of changes in the form of discontinuities in the structure leads to a modification of the simple stress distribution over the cross-section or over a localized volume of the component so that a local stress concentration is produced. This results in complex uniaxial, biaxial or even triaxial stresses, with the stress peak located at the root of the notch and its value decreasing towards the depth of the body [4–6]. Sources of increasing stress concentration are referred to as stress concentrators or generally notches. Notches can generally be divided into several basic groups:

- Structural notches, determined by shape and geometric changes in bodies in the form of offsets, recesses, grooves, threads, holes, etc.;
- Technological notches, determined by the properties of the surface layer of the material after chemical, thermal or mechanical processing, where a special role is played by transitions between the resulting different material structures, traces of chip machining, stamped markings, grooves, etc.;
- Metallurgical notches, associated with heterogeneity and anisotropy of the material resulting from disturbances of the internal structure of the material (dislocations, vacancies, scratches, etc.);
- Notches formed during the operation of the material due to aggressive environment (corrosion) or wear (grooves, scratches) [7].

Of the types of notches mentioned, only structural notches are desirable from a functional point of view. However, from a design and operational point of view, all stress concentrators are undesirable. To a large extent, they negatively affect the service life of the component and reduce its resistance to fatigue failure [8], because fatigue cracks initiate at the locations of local stress increase [9].

Stress and strain analysis in the notch region is quite a challenging discipline. Historically, the regularities of stress changes with the notch region began to be more seriously addressed in the 1930s by Neuber. However, this problem was addressed only at the level of simple structural elements.

In this paper, according to Figure 1, 6 shape-discontinuity-dimension-load configurations are considered:

- (a) Axially symmetric 3-dimensional stepped tension bar of circular cross-section with shoulder fillet.
- (b) A 2-dimensional stepped flat tension bar with shoulder fillet.

- (c) Axially symmetric 3-dimensional tension bar of circular cross-section with a U-shaped groove.
- (d) A 2-dimensional flat tension bar with opposite U-shaped notches.
- (e) A 2-dimensional infinitely wide thin flat body with opposite deep hyperbolic notches in tension.
- (f) A 3-dimensional infinitely wide body with deep hyperbolic groove in tension.

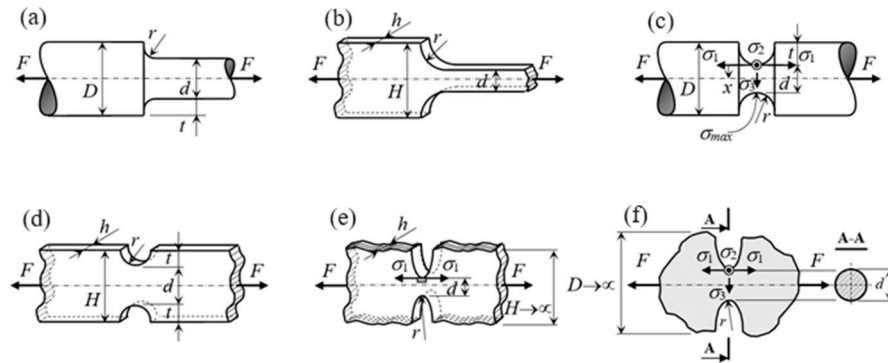


**Figure 1.** The 6 configurations of shape-discontinuity-dimension-load stress concentrators identifiable as (a–f).

### 3. Description of the Notch Effect

The so-called dimensionless stress concentration factor  $\alpha$ , also called form factor, is used to describe the notching effect. Two kinds of stress concentration factors can be distinguished. In the technical literature, it is most commonly defined as the ratio of the local maximum stress  $\sigma_{max}$ , e.g., at the root of the notch and the nominal (mean, average) stress value  $\sigma_{nom}$  in the weakened cross-section, according to the equation

$$\alpha = \frac{\sigma_{max}}{\sigma_{nom}}. \tag{1}$$

However, there is some inconsistency in practice when applying the value of the nominal stress to consider its value in the unweakened cross-section. However, this difference may disappear if the dimensions of the notch are small compared to the overall cross-sectional dimensions. The stress concentration factor takes into account the stress increase induced by the change in the local geometry of the body as well as the effect of detailed changes in the force flux in the cross-section. In general terms, however, the factor is related to the stress component that gives it the largest value. It is therefore sometimes referred to by indices of principal stress, e.g.,

$$\alpha_1 = \frac{(\sigma_{max})_1}{\sigma_{nom}}. \tag{2}$$

In the case of uniaxial tension, e.g., in the case of circular cross-sections of diameter  $d$  subjected to a tensile force  $F$ , the nominal tension itself will be expressed by the relation

$$\sigma_{nom} = (\sigma_{nom})_1 = \frac{4F}{\pi \cdot d^2}. \tag{3}$$

In the case of complex loading of the component where multi-axial stresses are assumed, it is appropriate to consider transforming the stress components into an equivalent uniaxial stress,

$$(\sigma_{max})_{eq} = \nu \cdot (\sigma_{max})_1, \tag{4}$$

which introduces the equivalent stress and the associated equivalent stress concentration factor into the calculation

$$\alpha_{\text{eq}} = \frac{(\sigma_{\text{max}})_{\text{eq}}}{\sigma_{\text{nom}}} = \nu \cdot \alpha_1. \quad (5)$$

$\nu$  is a dimensionless stress coefficient (factor) dependent on the ratio of the stress components at the most stressed location and on the strength hypothesis considered. For example, according to the von Mises hypothesis, which can be used in the case of minimal plastic deformation occurring, with a simple type of loading, not considering relaxation processes in a triaxial tension with a triad of principal stresses  $\sigma_1 > \sigma_2 > \sigma_3$ , the coefficient  $\nu$  can be expressed according to the relation

$$\nu^{\text{VM}} = \frac{(\sigma_{\text{max}})_{\text{eq}}^{\text{VM}}}{\sigma_1} = \frac{\sqrt{\sigma_1^2 + \sigma_2^2 + \sigma_3^2 - \sigma_1\sigma_2 - \sigma_2\sigma_3 - \sigma_3\sigma_1}}{\sigma_1}. \quad (6)$$

In the case of this hypothesis and considering the biaxial tension ( $\sigma_3 = 0$ ), this coefficient is determined by

$$\nu^{\text{VM}} = \sqrt{1 - \frac{\sigma_2}{\sigma_1} + \left(\frac{\sigma_2}{\sigma_1}\right)^2}. \quad (7)$$

The theoretical stress concentration factor related to an ideally elastic material generally corresponds to a higher stress concentration than actually occurs in the element due to the initiation of local plastic deformations. For this reason, the so-called effective stress concentration factor, which is equivalent to the effective notch factor, is introduced. With more significant plastic deformations, the shape of the notch already changes and the stress reduction is already significant. In practice, the resulting stress–strain state can be expressed analytically by the so-called Neuber rule, which, among other things, relates the stress concentration factor to the deformation. However, this rule loses accuracy with increasing degree of plasticization [10,11].

#### 4. Stress Concentration Induced by a Change in Cross-Sectional Area

In technical engineering practice, one of the most common forms of stress concentration are the locations of sudden changes in the shapes and especially the sizes of the cross-sectional areas. Such concentrators mainly concern bars, shafts and beams with tensile, torsional and bending stresses and often providing functional movement. When designing them, it is necessary to take into account not only the method of stressing but also to ensure that it is functional and can be assembled into a system. The design of such structural elements and their frequent cross-sectional changes are thus subject to many design constraints arising from the location of bearings, pulleys, gears and other structural elements. From the point of view of the magnitude of stress concentration, the most unfavorable condition is that of sharp transitions between cross-sections. The corresponding stress in such a notch is then greater the more significant the change in cross-section [12,13].

The design of the transition method between shaft sections with different diameters depends on whether an additional structural element is applied at a given location or whether the geometry of the critical region can be varied within a certain range. Historically, the sharp transition was initially replaced by a constant radius rounded transition. In order to reduce stress concentration to the smallest possible level, this radius is chosen to be as large as possible [13–15]. However, further experimental and numerical analyses have shown that more significant peak stress reduction can be achieved by complex rounding with variable radii. Such optimization of the transition curve can then lead to elliptical, parabolic or other more complex shapes [6,16]. However, this approach requires case-by-case optimization. The technological handling of more complex transitions can also pose problems. Last but not least, such a solution must also satisfy the intended design layout. For example, the transition radius must be smaller than the radius of curvature of the edge of, e.g., the inner ring of the bearing. However, the size of the radius may already be so

small that it may not be sufficient for the necessary peak stress reduction. In such a case, a more optimization, design and technology-intensive solution is required, using, e.g., relief grooves [6,17].

### 5. The Problem of Determining Stress Concentration Factors

The fundamental problem of determining stress concentration factors is the creation or existence of a certain system solution for their fast, simple and efficient determination. This is particularly relevant not only for existing, but also for new mutual configurations or combinations of shape, dimension and loading. The results are most often represented graphically, i.e., by tables, diagrams or nomograms. It is also possible to express them analytically by means of appropriate dependencies or equations. Among the more widespread methods, methods based on experimental and numerical analyses, or combinations thereof, may be mentioned. Whatever the approach used, however, the important criterion must be to achieve acceptable precision and, at the same time, efficiency and statistical significance.

Experimental methods are mainly dominated by methods based on transmission photoelasticity. However, a particular problem with this method is that the stress analysis of a certain group of objects, due to the evaluation methodology, is made difficult or complicated by complex stress states. These are situations where, depending on the shape-discontinuity-dimensions-load configuration, the stresses may be not only uniaxial but also biaxial and in some cases even triaxial. In the case of triaxial strain, the application of spatial photoelasticity would be required, but this is a rather labor-intensive and challenging procedure. The reflection method (Photostress<sup>®</sup>) is much less suitable for these situations. A relatively unsuitable method for such cases is the strain-gauge method, which is a fairly widespread and well-established method in other stress analysis cases. The inappropriateness of this method lies in the applied principle of measuring small deformations and the consequent inability to capture large stress and strain gradients in the conditions of small stress concentrator regions. Moreover, the situation is more complex, e.g., in the case of 3D axially symmetric and other objects. In this case, it is particularly challenging to obtain data on the gradients of the quantities of interest, and the problem is not only related to the strain-gauge method, but also to reflection photoelasticity. However, any applied experimental method requires, in addition to the respective hardware and software means of the measurement chains, mainly a corresponding physical model as a material object for each shape-discontinuity-dimension-stress configuration separately. But then such procedures are unacceptably time-consuming and economically demanding. Some advances in the creation of physical models for these purposes can be brought about by modern additive 3D printing technologies.

Rotationally symmetric and spatially symmetric objects, e.g., according to Figure 1c are typical examples of objects with a complex stress state. According to our classification, they are axially symmetric 3-dimensional tension bar of circular cross-section with a U-shaped groove. In this case, the largest increase in stress from the nominal value  $(\sigma_{\text{nom}})_1$  occurs at the root of the notch, assuming perfectly elastic tension at all points along the perimeter of the cross-section. This maximum stress has a perpendicular direction to the smallest cross-section of the bar. This is the axial stress  $(\sigma_{\text{max}})_1$  denoted by the index 1. At the root of the notch for  $x = 0$ , in addition to this stress, there is a peak circumferential stress of magnitude  $(\sigma_{\text{max}})_2$ . If the free unloaded surface of the root of the notch is assumed, then the third principal stress in the direction of the radius of the bar, i.e., in the radial direction, is zero ( $\sigma_3 = 0$ ). This location is then corresponded by the corresponding equivalent stress concentration factor  $\alpha_{\text{eq}}$  and stress factor  $\nu_{(x=0)}$ . However, the stress factor varies from location to location. For the surface of the notch where biaxial tension is assumed, it is possible to write  $\nu_{(x=0)} = \nu_{\text{II}}$ . Below the surface of the notch towards the inside of the bar for  $x > 0$ , the tension is triaxial, so in general  $\nu_{(x>0)} = \nu_{\text{III}}$ . The progression of the individual principal stresses and the equivalent stress according to von Mises theory for this configuration is shown in Figure 2.

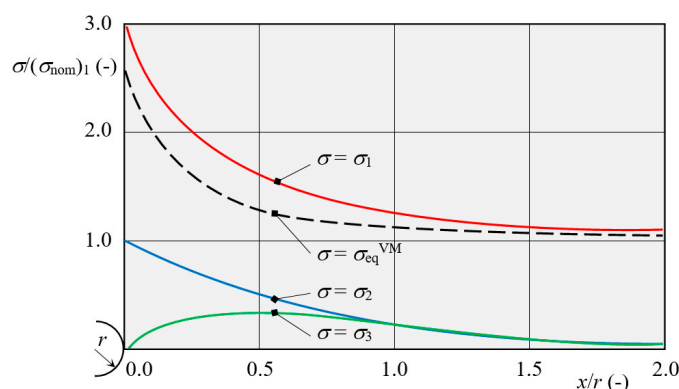


**Figure 2.** The course of the individual relative principal stresses and equivalent von Mises stresses for the shape configuration (c) in the smallest cross-section as a function of the dimensionless parameter  $x/r$ .

In this case, the greatest concentration of equivalent stresses is at the surface of the bar at the root of the notch. However, for a different notch shape, the largest value of equivalent stress is located below the surface of the root of the notch. During cyclic loading, it is at these locations that the first fatigue damage and fatigue cracks may occur.

Among the numerical solutions for the determination of the stress concentration factors, the finite and boundary element methods (FEM and BEM) can be mainly included. Numerical solutions require, of course, in addition to powerful and stable hardware and software resources, first of all the creation of numerical models. An important factor in numerical solutions is the question of the method, quality and detail of the meshing, or finite or boundary element generation. It is a question of applying a kind of trade-off between simplicity and speed of solution on the one hand and the achieved accuracy and statistical significance on the other hand.

In practice, hybrid or combined approaches (solutions) are also applied. One example is the experimental-approximation transformation approach. Since the stresses of 3D—axis(rotationally)symmetric versions—are considerably more difficult to analyze experimentally, e.g., by the transmission Photostress<sup>®</sup> method, than those of 2D—flat versions—a combined approach is chosen. Its essence is that the strain of the 2D version is experimentally investigated and this is then approximated or transformed to the 3D version using known and validated approximation relations. Such an approach may not give the most accurate results, but is relatively fast and efficient.

Thus, for example, the experimentally obtained value of  $\alpha_d$  for the 2D dimensionally finite flat version of the shape configuration (d) is approximated to  $\alpha_c$  for the 3D dimensionally finite rotationally symmetric version of the shape configuration (c) by multiplying by the fraction of the values of  $\alpha_f$  and  $\alpha_e$  according to

$$\alpha_c = \alpha_d \frac{\alpha_f}{\alpha_e}, \tag{8}$$

where  $\alpha_e$  and  $\alpha_f$  are experimentally obtained stress concentration factors with dependence on dimensionless  $r/d$  ratios according to Figure 3.  $\alpha_e$  is the factor for the 2D dimensionally infinite flat version of the shape configuration (e) and  $\alpha_f$  is the factor for the 3D dimensionally infinite rotationally symmetric version of the shape configuration (f). The dependence of each of the quantities  $\alpha_e$  and  $\alpha_f$  is shown in Figure 3 by a pair of curves belonging to two different ranges of  $\alpha$  values and two different  $r/d$  ratio ranges. The affiliation of the curve to one of the two pairs of scales is indicated by arrows—either to the right and up or to the left and down. The dependencies for  $\alpha_f$  for the left and bottom scales are given for three values of the Poisson ratio  $\mu$ .

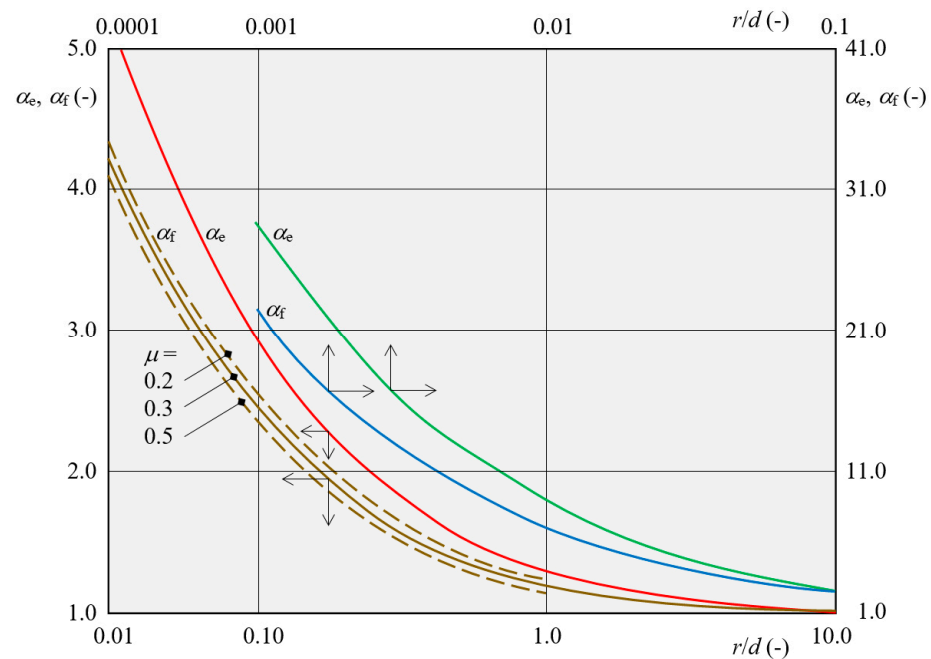


**Figure 3.** Experimentally obtained stress concentration factors  $\alpha_e$  and  $\alpha_f$  with dependence on dimensionless  $r/d$  ratios.

Similarly, it is possible to recalculate the experimentally obtained value  $\alpha_b$  for the 2D dimensionally finite flat version of the shape configuration (b) to  $\alpha_a$  for the 3D dimensionally finite rotationally symmetric version of the shape configuration (a) according to

$$\alpha_a = \alpha_b \frac{\alpha_f}{\alpha_e} \tag{9}$$

The courses of the  $\alpha_b$  and  $\alpha_a$  factors as a function of the dimensionless ratios  $r/d$  and  $D/d$  or  $H/d$ , respectively, are shown in Figures 4 and 5. Diagrams in Figures 2–5 were created based on the literature [18].

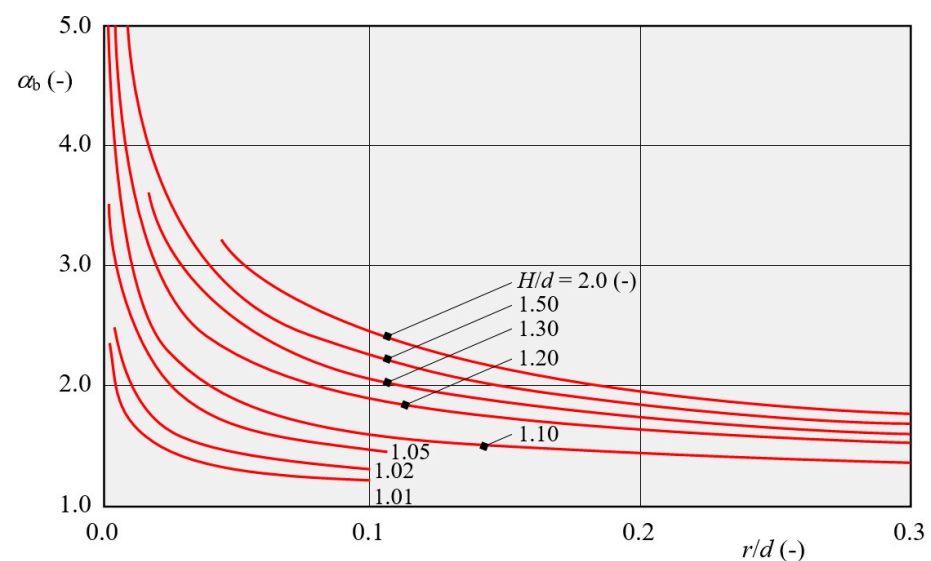


**Figure 4.** Experimentally obtained stress concentration factor  $\alpha_b$  with dependence on dimensionless ratios  $r/d$  and  $H/d$ .

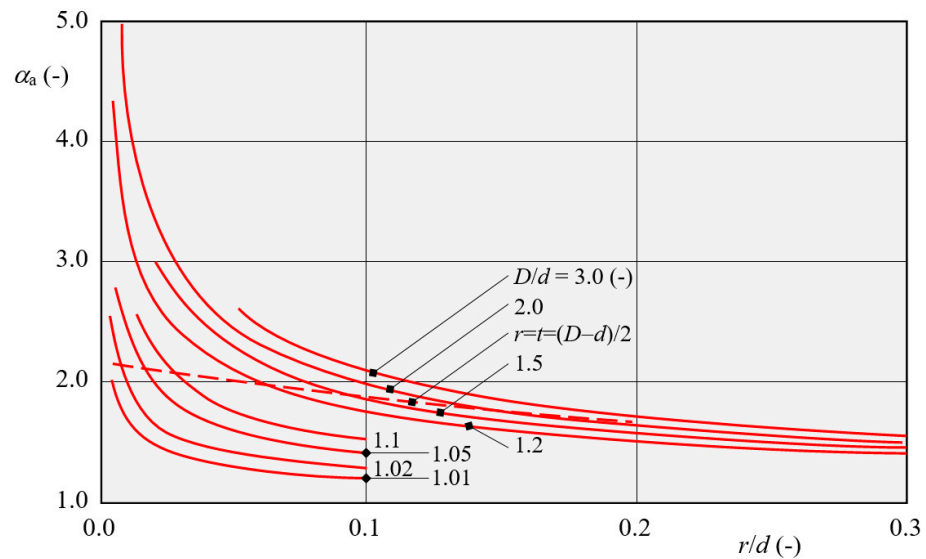


**Figure 5.** Stress concentration factor  $\alpha_a$  obtained by transformation from 2D to 3D with dependence on dimensionless ratios  $r/d$  and  $D/d$ .

The correlation of the individual factors  $\alpha_a, \alpha_b, \alpha_c, \alpha_d, \alpha_e,$  and  $\alpha_f$  of the 2D shape configurations (b), (d), (e) and 3D shape configurations (a), (c), (f) of the tensile stress concentrators of Figure 1 can also be expressed by the symbolic proportion diagram of Figure 6. The validity of the above relations has been partially verified experimentally and numerically not only for tensile loading but also for torsion and bending loading.

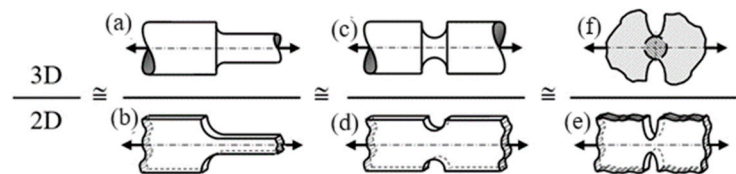


**Figure 6.** Correlation of stress concentration factors  $\alpha_a, \alpha_b, \alpha_c, \alpha_d, \alpha_e,$  and  $\alpha_f$  in symbolic proportion for 2D and 3D shape configurations.

The graphical representation  $\alpha_a$  of Figure 5 is complemented or expressed also by analytical approximations depending on the dimensionless  $2t/D$  ratio according to [15]

$$\alpha_{Ct} = c_3 \left(\frac{2t}{D}\right)^3 + c_2 \left(\frac{2t}{D}\right)^2 + c_1 \left(\frac{2t}{D}\right)^1 + c_0 \left(\frac{2t}{D}\right)^0. \tag{10}$$

The quantity  $t$  was expressed on the basis of the relation

$$t = \frac{D - d}{2}. \tag{11}$$

The individual dimensionless coefficients of  $c_i$  are expressed based on the dimensionless  $t/r$  ratio according to the relations in Table 1.

To determine the values of  $\alpha_a$  for the shape configuration (a) Tipton [18] based on FEM analyses offers analytical dependence in shape

$$\alpha_{Ti} = 0.493 + 0.48 \left(\frac{D}{d}\right)^{-2.43} + \left(\frac{r}{d}\right)^{-0.48} \cdot \sqrt{\frac{3.43 - 3.41 (D/d)^2 + 0.0232 (D/d)^4}{1 - 8.85 (D/d)^2 - 0.078 (D/d)^4}}. \tag{12}$$

The relationship is recommended by Tipton and applicable to a wide range of dimensionless parameter ratios  $0.002 \leq r/d \leq 0.3$  and  $1.01 \leq D/d \leq 6.0$ .

**Table 1.** Dimensionless coefficients  $c_i$  as functions of dimensionless  $t/r$  ratios to determine stress concentration factors according to relation (10).

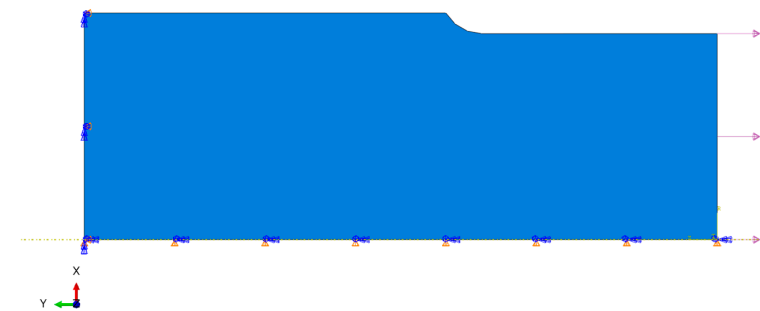
	$0.1 \leq t/r \leq 2.0$	$2.0 \leq t/r \leq 20.0$
$c_3$	$0.365 - 2.098\sqrt{t/r} + 0.878t/r$	$-0.593 - 0.028\sqrt{t/r} - 0.106t/r$
$c_2$	$-0.302 + 3.977\sqrt{t/r} - 1.744t/r$	$2.198 - 0.486\sqrt{t/r} + 0.165t/r$
$c_1$	$0.012 - 3.036\sqrt{t/r} + 0.961t/r$	$-1.805 - 0.346\sqrt{t/r} - 0.038t/r$
$c_0$	$0.926 + 1.157\sqrt{t/r} - 0.099t/r$	$1.200 + 0.860\sqrt{t/r} - 0.022t/r$

## 6. Stress FEM Analysis of Shape-Discontinuity-Dimensions-Load Configuration (a)

The subject of numerical stress analyses for subsequent comparison and statistical evaluation was the shape-discontinuity-dimensions-load configuration (a) according to Figure 1. The overall dimensions were defined by a trio of parameters: the larger diameter  $D$ , the smaller diameter  $d$ , and the transition radius or the radius of curvature of the transition curve  $r$ .

The aim of the numerical analyses was to determine the nominal and maximum equivalent and principal normal stresses in the critical, i.e., transition region of the individual diameters. These should then be the main characteristic defining the peak stress of the notching effect. The data obtained were then used to express (quantify) the stress concentration factors for specific values of diameters  $D$ ,  $d$ , radius  $r$ , and ratios  $D/d$  and  $r/d$ , respectively, in the axial tension loading regime.

Since the FEM analysis of configuration (a) was the case of an axially loaded rotationally (axially)-symmetric element, the numerical modelling could be made more efficient by using a two-dimensional axisymmetric shell model with a longitudinal axis of rotation and with appropriate consideration of the configuration in the definition of the boundary conditions (Figure 7). The definition of the transition curve for the case  $t > r$  was implemented in the form of a circular arc with radius  $r$  passing through the edge of the larger shaft cross-section and tangent to diameter  $d$ . In the other cases, the circular arc took the form of a tangent to the respective edges.

**Figure 7.** Boundary conditions and loading used for finite element analysis.

The appropriate working values for the  $D/d$  and  $r/d$  ratios and their intercombinations were chosen to ensure that the analyses included the full applicable range of dependencies for the stress concentration factors imported from the other sources being compared. Another important criterion was to maintain a certain minimum statistical significance of the obtained results but without a huge increase in the number of individual simulations required.

Based on these criteria, 4 individual  $r/d$  ratios with values of 0.01, 0.05, 0.08 and 1.10 were selected for the 4 individual selected  $D/d$  ratios with values of 1.01, 1.02, 1.05 and 1.10, respectively. Similarly, for 4 individual selected  $D/d$  ratios with values of 1.2, 1.5, 2.0 and 3.0, 4 individual  $r/d$  ratios were selected with values of 0.01, 0.05, 0.08 and 1.10. This provided the basis for  $2 \times 4 \times 4 = 32$  combinations of input data. For the selected  $D/d$  and  $r/d$  ratios and the selected diameter size value  $D = 50$  mm, the  $d$  and  $r$  values were

expressed to 3 decimal places in the next step. For each such case, a separate geometric model of the shaft was then generated, made as an axisymmetric shell element with a longitudinal axis of rotation.

In the range of elastic deformations, the stress concentration factors were assumed to be independent of the material characteristics (properties) and the magnitude of the load, assuming isotropy of the material properties. The material considered was a standard steel, with the following characteristics: Young's modulus  $E = 210$  GPa and Poisson's ratio  $\mu = 0.3$ .

For all combinations of  $D/d$  and  $r/d$  ratios, the model was loaded by a single force  $F = 2$  kN applied axially in the direction of the longitudinal axis of the element (shaft). The model is loaded by tensile forces.

Since the results of numerical simulations are mainly influenced by the quality and size of the finite elements, it was advisable to define the location of the transition curve with the smallest possible elements. In this case, an element size of 0.25 mm was chosen for the investigated region.

For the needs of local refinement of the mesh, a non-uniform distribution of elements along the edges of the model was chosen. Along the curve and its transition to a small shaft radius, a fixed size of 0.25 mm was defined, and towards both ends of the shaft, a bias function was used to determine the element size, which prescribed an increase in element size from 0.25 mm to 4.0 mm with an increasing tendency towards the edge. The critical region investigated was 8 layers of elements interleaved with a regular arrangement towards the volume of the component. Although the choice of finite element type may not have a significant effect on the accuracy of the results, a more regular arrangement of the grid elements was achieved solely by the choice of four-node quadratic elements. Quadratic quadrilateral elements of type CAX8R were used for discretization and the FEM analysis was performed in the ABAQUS programming environment.

In total, several dozen models were created for different combinations of  $D/d$  and  $r/d$  ratios. In order to increase the accuracy of the analysis, it was necessary to make adequate adjustments to the FE mesh for each numerical model, while ensuring the regularity of the arrangement of the elements in the investigated region. The final choice of the element size while gradually reducing the element size was completed at the stage when a negligible change in stress had already been achieved by the previous refinement of the mesh. The main monitored output of each simulation was the maximum normal stresses identified at the point of intersection of adjacent diameters. The maximum values of the equivalent stresses  $\sigma_{VM}$  according to the von Mises theory and the principal normal stresses  $\sigma_1$  in the longitudinal axis direction, i.e., in the direction of the applied loading force  $F$ , were monitored.

The many results obtained from FEM analyses are illustrated by several examples in Figures 8–11. Figure 8 shows the equivalent stress field according to the von Mises theory on a quarter 3D model with a close-up of the 2D view in Figure 9 at the location of the transition arc. Figure 10 shows the field of principal normal stresses in the longitudinal axis direction on the quarter 3D model with detail in Figure 11 in 2D view at the location of the transition arc.

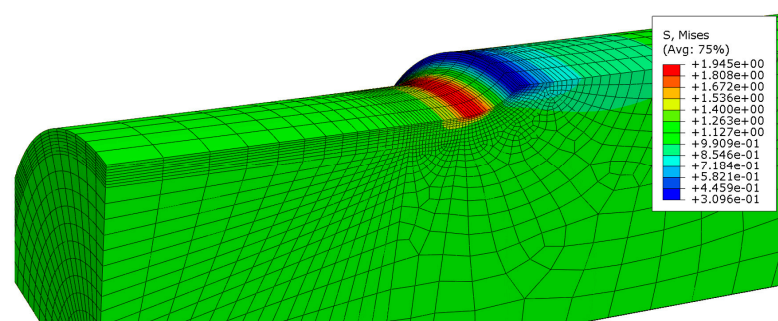


**Figure 8.** Example of a equivalent stress field according to von Mises theory on a quarter 3D model.

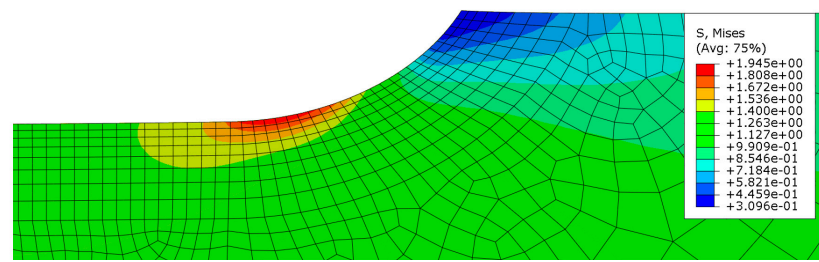


**Figure 9.** Example of the detail of the equivalent stress field according to von Mises theory in 2D view at the location of the transition arc.

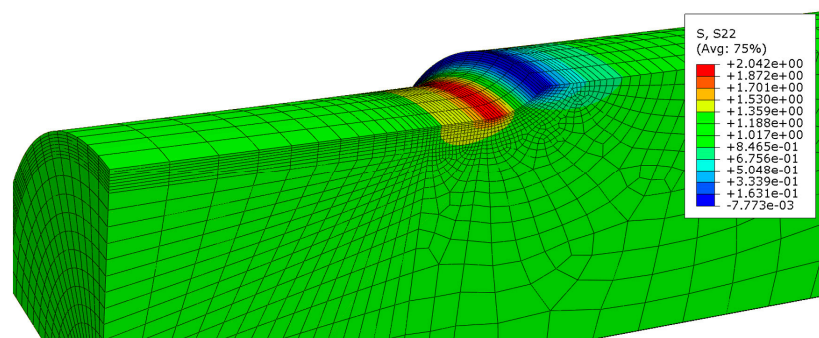


**Figure 10.** Example of the principal normal stress field in the longitudinal axis direction on a quarter 3D model.

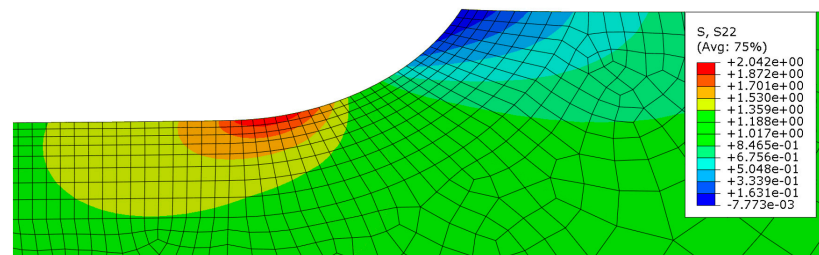


**Figure 11.** Example of the detail of the principal normal stress field in the longitudinal axis direction in 2D view at the location of the transition arc.

### 7. Regression and Correlation Analysis of Stress Concentration Factor Values Obtained from FEM Analysis

Based on the values of the normal stresses  $\sigma_{VM}$  and  $\sigma_1$  obtained by FEM analysis, the stress concentration factors  $\alpha_{VM}$  and  $\alpha_{S1}$  were then expressed by dividing the corresponding stresses and  $\sigma_{VM}$ ,  $\sigma_1$ , respectively, by the corresponding nominal value  $\sigma_{nom}$  according to the relations

$$\alpha_{VM} = \frac{\sigma_{VM}}{\sigma_{nom}}, \alpha_{S1} = \frac{\sigma_1}{\sigma_{nom}}. \tag{13}$$

For the purpose of comparison of the data thus obtained, the values of the stress concentration factors of  $\alpha_{Ct}$  and  $\alpha_{Ti}$  from the imported sources were expressed in parallel. The concentration factor of  $\alpha_{Ct}$  was obtained by applying the graphical basis of Figure 5 and the corresponding analytical dependence (10), respectively, and the corresponding concentration factors of Table 1. The concentration factor  $\alpha_{Ti}$  was obtained by applying the analytical dependence (12). For each of the  $8\alpha_{VM}$  dependencies, a regression analysis was simultaneously performed to replace these dependencies with analytical functions by a triplet of regression models P3, P2, and Pw and the corresponding trend lines TL1, TL2, and TL3, respectively. The chosen replacement was by the 3rd-degree polynomial of P3 according to relation (14), the 2nd-degree polynomial of P2 according to relation (15)

and the power function of Pw according to relation (16). All models are expressed by the functional dependence on the dimensionless parameter  $r/d$

$$\alpha_{VMP3} = b_3 \left(\frac{r}{d}\right)^3 + b_2 \left(\frac{r}{d}\right)^2 + b_1 \left(\frac{r}{d}\right)^1 + b_0 \left(\frac{r}{d}\right)^0, \tag{14}$$

$$\alpha_{VMP2} = b_2 \left(\frac{r}{d}\right)^2 + b_1 \left(\frac{r}{d}\right)^1 + b_0 \left(\frac{r}{d}\right)^0, \tag{15}$$

$$\alpha_{VMPw} = b_1 \left(\frac{r}{d}\right)^{b_0}. \tag{16}$$

The values of regression coefficients  $b_3, b_2, b_1,$  and  $b_0$  obtained by regression analysis for individual regression models represented by regression functions P3, P2, and Pw for  $D/d$  ratios are shown in Table 2. At the same time, the values of the coefficient of determination  $R^2$  are also given. The regression and stress analysis was performed in the MS Excel software environment as a part of Microsoft Office 2013 Professional Plus.

**Table 2.** Regression coefficients  $b_3, b_2, b_1,$  and  $b_0$  and coefficients of determination  $R^2$  as a functions of  $D/d$  ratios of individual regression models.

$D/d$	Regression f.	$b_3$	$b_2$	$b_1$	$b_0$	$R^2$
[-]	(Trend line)	[-]	[-]	[-]	[-]	[-]
1.01	Polynomial P3°	-981.50	241.780	-20.9200	1.8664	1.0000
	Polynomial P2°	x	77.795	-13.6090	1.8047	0.9932
	Power Pw	x	x	0.8575	-0.1450	0.9938
1.02	Polynomial P3°	-1154.10	304.120	-27.9510	2.1979	1.0000
	Polynomial P2°	x	111.300	-19.3550	2.1254	0.9952
	Power Pw	x	x	0.8323	-0.1830	0.9944
1.05	Polynomial P3°	-2991.90	547.620	-46.3450	2.8687	1.0000
	Polynomial P2°	x	164.690	-29.2720	2.7247	0.9923
	Power Pw	x	x	0.8101	-0.2400	0.9978
1.10	Polynomial P3°	-2870.70	720.840	-63.3570	3.5802	1.0000
	Polynomial P2°	x	241.200	-41.9730	3.3999	0.9938
	Power Pw	x	x	0.8084	-0.2840	0.9971
1.20	Polynomial P3°	-138.63	79.631	-16.5140	2.7220	1.0000
	Polynomial P2°	x	19.139	-9.0341	2.4705	0.9937
	Power Pw	x	x	0.9934	-0.2440	0.9974
1.50	Polynomial P3°	-221.08	124.970	-25.1040	3.3938	1.0000
	Polynomial P2°	x	28.496	-13.1760	2.9928	0.9919
	Power Pw	x	x	0.9489	-0.3100	0.9967
2.00	Polynomial P3°	-266.22	149.270	-29.6360	3.7337	1.0000
	Polynomial P2°	x	33.107	-15.2720	3.2509	0.9912
	Power Pw	x	x	0.9197	-0.3420	0.9972
3.00	Polynomial P3°	-275.25	154.790	-30.9020	3.8487	1.000
	Polynomial P2°	x	34.679	-16.0510	3.3495	0.9916
	Power Pw	x	x	0.9038	-0.3570	0.9980

The resulting courses of concentration factors  $\alpha_{Cl}, \alpha_{VM}, \alpha_{VMP3}, \alpha_{VMP2}, \alpha_{VMPw}, \alpha_{S1}$  and  $\alpha_{Ti}$  as functions of the dimensionless ratios  $r/d$  for certain specific values of the dimensionless ratios  $D/d$  are jointly plotted in Figures 12–14, respectively—Figure 12 for  $D/d$  ratios of 1.01, 1.02, 1.05 and 1.10, Figure 13 for  $D/d$  ratios of 1.2 and 2.0 and Figure 14 for  $D/d$  ratios of 1.5 and 3.0.

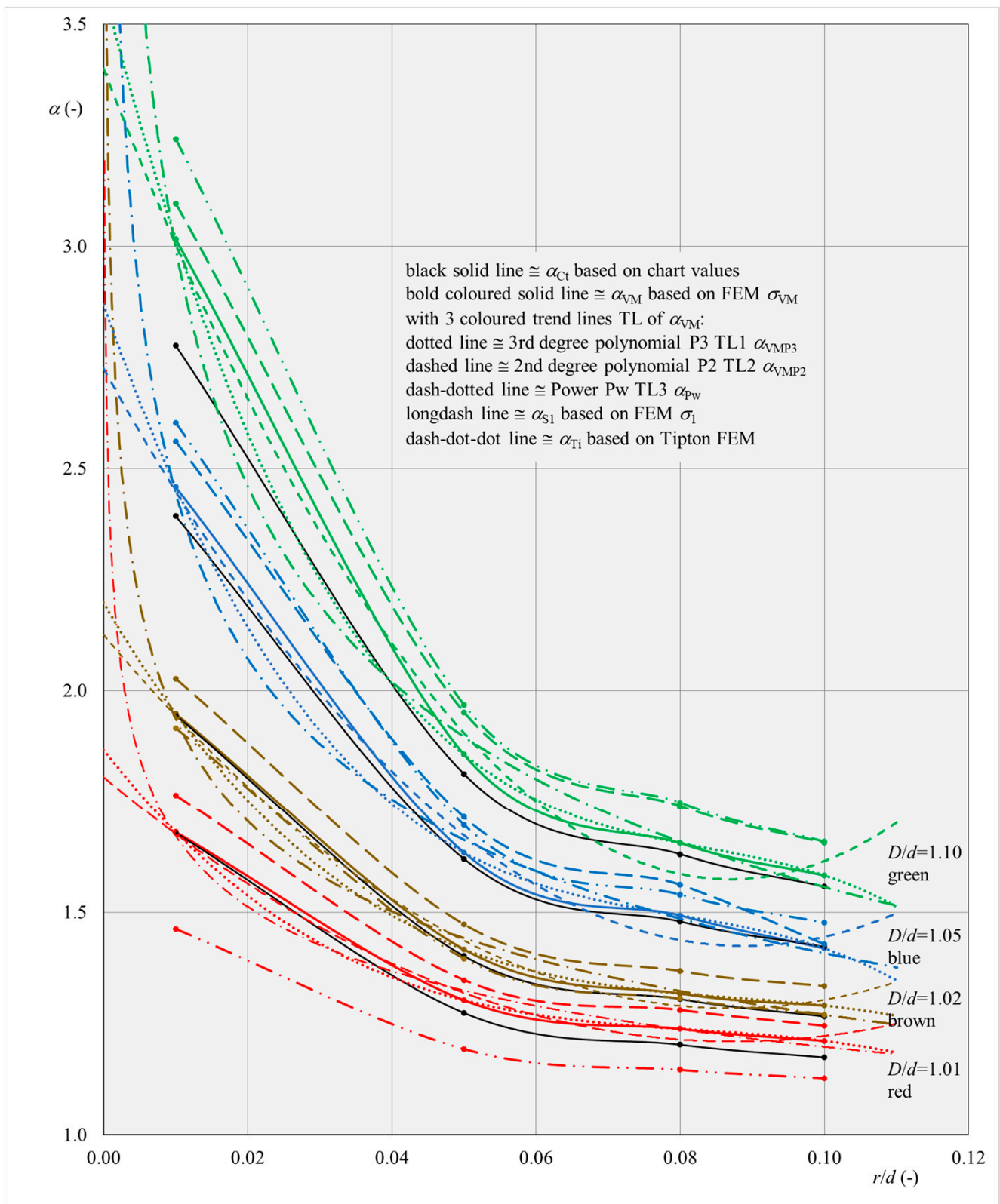


**Figure 12.** Plots of the concentration factors  $\alpha_{Ct}$ ,  $\alpha_{VM}$ ,  $\alpha_{VMP3}$ ,  $\alpha_{VMP2}$ ,  $\alpha_{VMPw}$ ,  $\alpha_{S1}$  and  $\alpha_{Ti}$  as functions of dimensionless  $r/d$  ratios for dimensionless  $D/d$  ratios of 1.01, 1.02, 1.05 and 1.10.

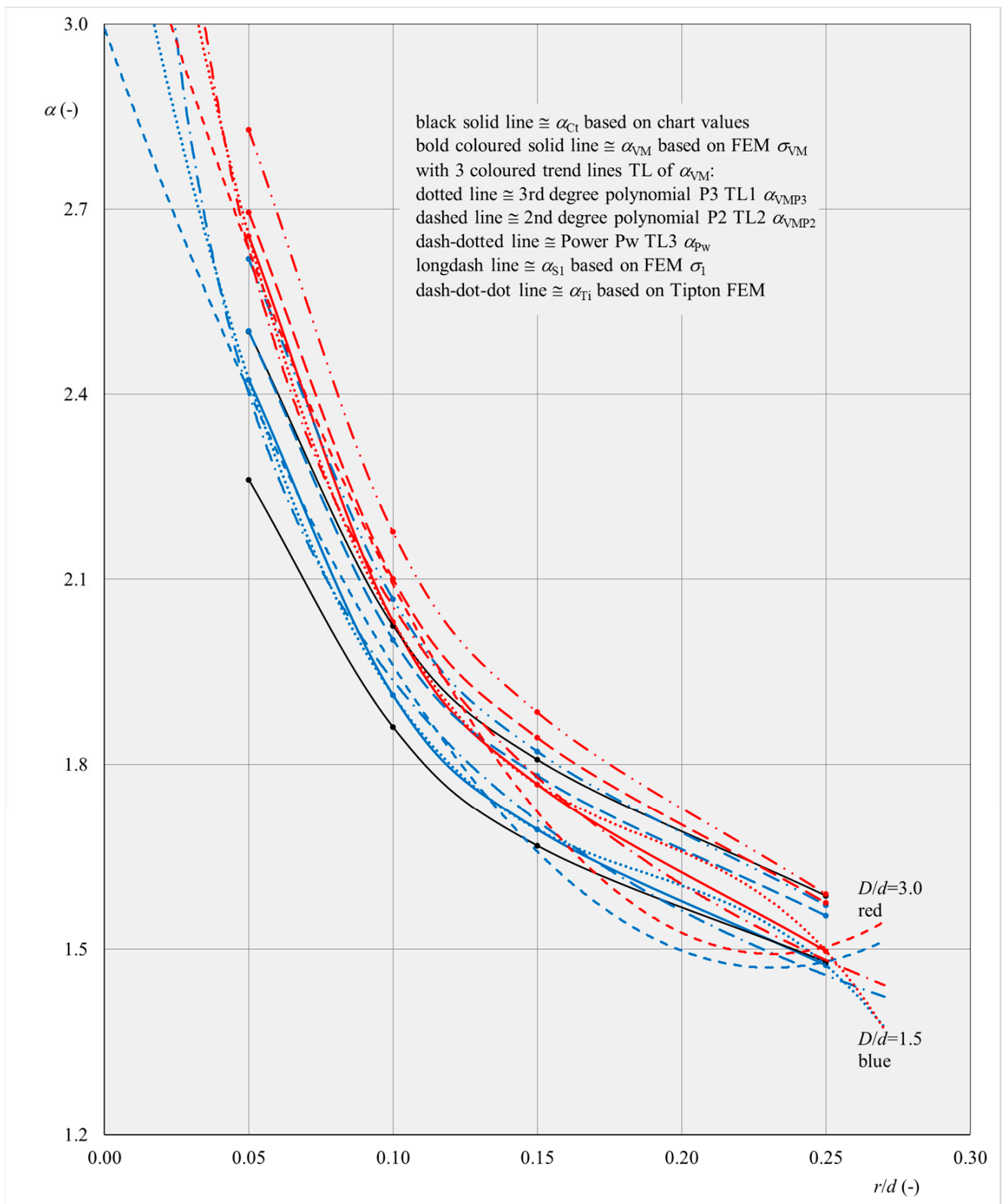


**Figure 13.** Plots of the concentration factors  $\alpha_{Ct}$ ,  $\alpha_{VM}$ ,  $\alpha_{VMP3}$ ,  $\alpha_{VMP2}$ ,  $\alpha_{VMPw}$ ,  $\alpha_{S1}$  and  $\alpha_{Ti}$  as functions of dimensionless  $r/d$  ratios for dimensionless  $D/d$  ratios of 1.2 and 2.0.

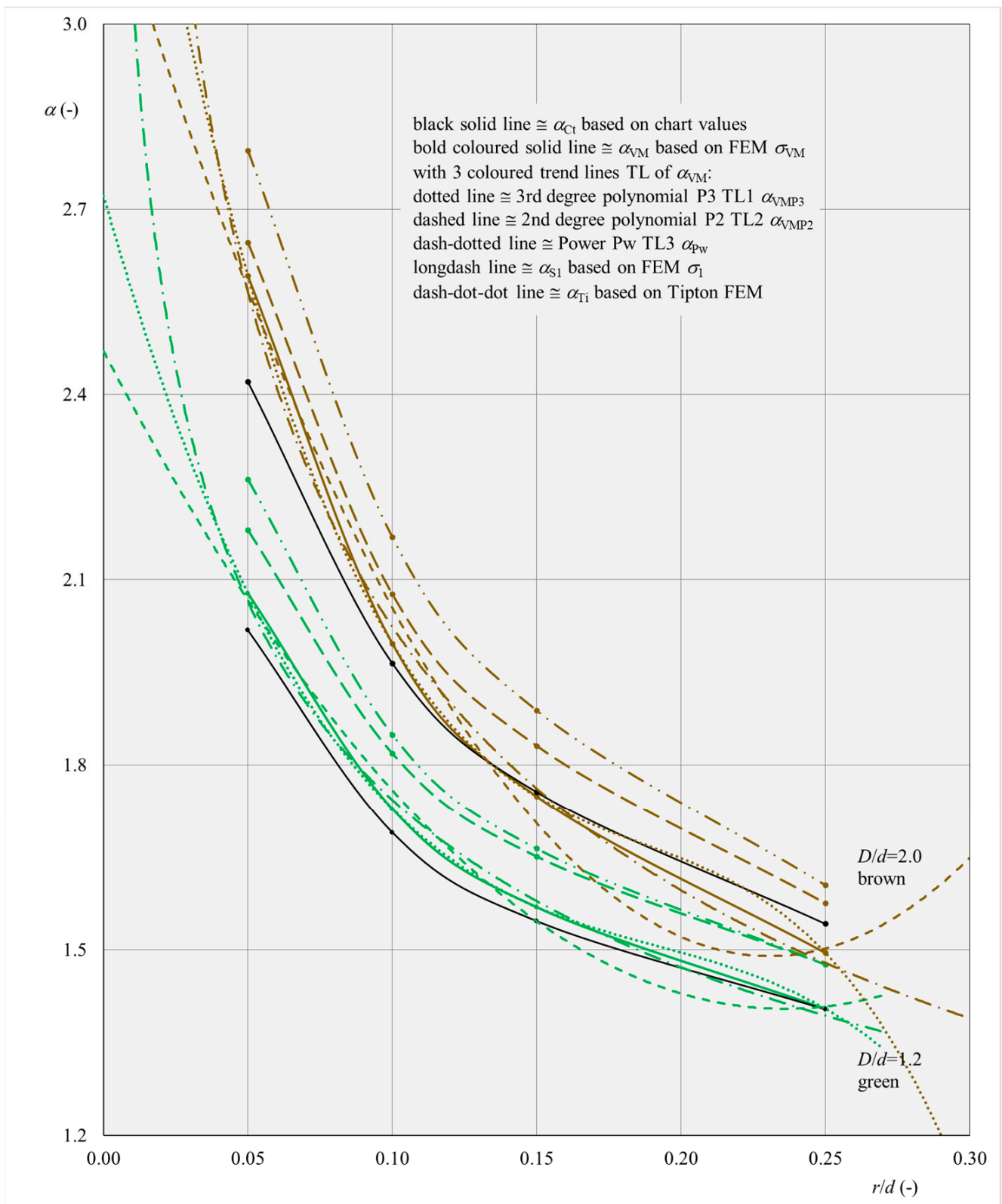


**Figure 14.** Plots of the concentration factors  $\alpha_{Ct}$ ,  $\alpha_{VM}$ ,  $\alpha_{VMP3}$ ,  $\alpha_{VMP2}$ ,  $\alpha_{VMPw}$ ,  $\alpha_{S1}$  and  $\alpha_{Ti}$  as functions of dimensionless  $r/d$  ratios for dimensionless  $D/d$  ratios of 1.5 and 3.0.

### 8. Mutual Comparison of Stress Concentration Factors Obtained from FEM Analyses and Stress Concentration Factors Imported from External Sources

In this section of the paper, a comparison is made between the values of the stress concentration factors  $\alpha_{VM}$  obtained by FEM analysis and the values  $\alpha_{Ct}$  and  $\alpha_{Ti}$  imported from external sources. The basic indicator will be the percentage difference  $\Delta\alpha_{Ct}$  and  $\Delta\alpha_{Ti}$  of the values of the concentration factors  $\alpha_{Ct}$  and  $\alpha_{Ti}$  compared to the reference value of the concentration factors  $\alpha_{VM}$  according to the relations

$$\Delta\alpha_{Ct} = \frac{\alpha_{Ct} - \alpha_{VM}}{\alpha_{VM}} \cdot 100 [\%], \Delta\alpha_{Ti} = \frac{\alpha_{Ti} - \alpha_{VM}}{\alpha_{VM}} \cdot 100 [\%] \tag{17}$$

The data thus obtained are graphically interpreted in the graphs in Figures 15 and 16. The percentage differences of  $\Delta\alpha_{Ct}$  and  $\Delta\alpha_{Ti}$  as a function of  $r/d$  for  $D/d$  ratios of 1.01, 1.02, 1.05 and 1.10 are shown in Figure 15 and for  $D/d$  ratios of 1.2, 1.5, 2.0 and 3.0 are shown in Figure 16.

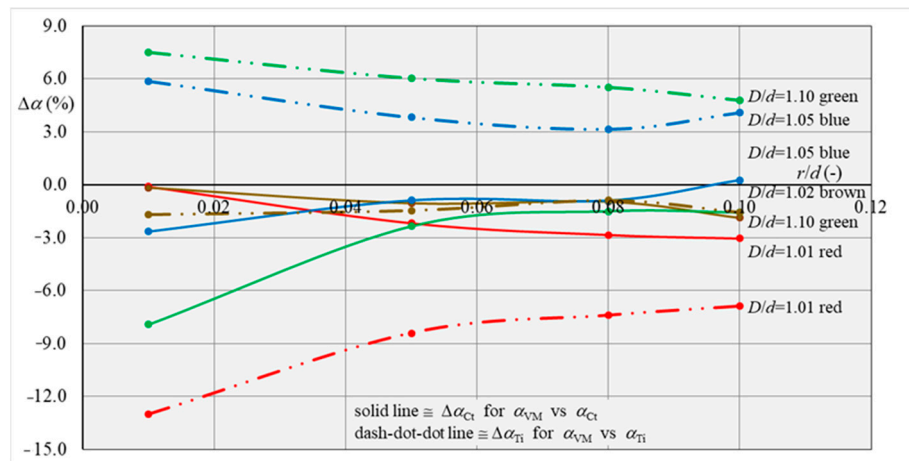


Figure 15. Graphical representation of the percentage differences of  $\Delta\alpha_{Ct}$  and  $\Delta\alpha_{Ti}$  as functions of  $r/d$  for  $D/d$  ratios of 1.01, 1.02, 1.05 and 1.10.

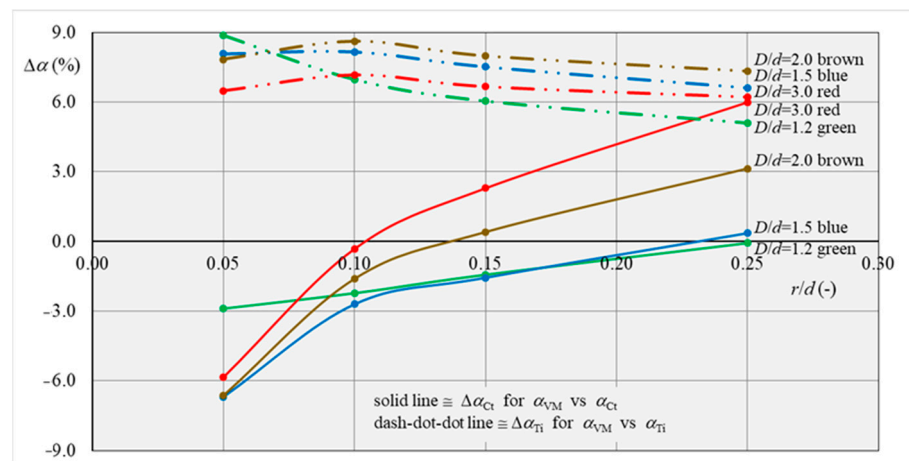


Figure 16. Graphical representation of the percentage differences of  $\Delta\alpha_{Ct}$  and  $\Delta\alpha_{Ti}$  as functions of  $r/d$  for  $D/d$  ratios of 1.2, 1.5, 2.0 and 3.0.

### 9. Summary Evaluation of the Analyses Performed and Results Obtained

#### 9.1. Evaluation of FEM Analyses

Based on the detailed evaluation of the FEM data, it can be concluded that the maximum values of the equivalent stresses  $\sigma_{VM}$  and the principal normal stresses  $\sigma_1$  are localized to the region of the transition curve connection to the surface of the shaft section with

diameter  $d$ . The maxima of the principal normal stresses show slightly higher values in the range of 2–3% compared to the equivalent stresses. In terms of stress distribution, the principal normal component shows a more significant representation of higher stress levels in the direction of the element volume, while at the same time, in contrast to the equivalent stresses, very slightly higher stress levels are observed throughout the shaft volume at the  $d$ -diameter level. In terms of the orientation of the principal normal stresses, tensile stresses dominate, except at the beginning of the transition curve where negligible compressive stresses are observed. The nominal values of the normal stresses  $\sigma_{nom}$  were expressed for a smaller circular cross-section with diameter  $d$  according to relation (3).

Due to the smooth transition of stress levels and the absence of abnormalities in the form of stress singularities, the choice of the finite element type and the method of discretization of the structure can be described as appropriate, in agreement with the conclusions in, e.g., [3].

### 9.2. Evaluation of Regression and Correlation Analyses

In all regression and correlation analyses performed, the value of determination  $R^2$ , which should capture the confidence level, was in the relatively high and narrow range of 0.991–1.000. This implies that each of the models within the terms of the analysis could be considered statistically acceptable, with a high level of confidence. The highest value of  $R^2 = 1.000$  belonged to all P3 regression models with a polynomial dependence of degree 3. However, based on a visual assessment of the degree of overlap of each regression curve with the original dependence for  $\alpha_{VM}$ , the power function Pw can be considered the most acceptable regression dependence for all cases. Its advantage over the polynomial dependencies P3 and P2 is also its relative simplicity. At the same time, the relatively small statistical sets, always containing 4 elements, can be mentioned as the main limiting factor in the analyses performed.

A number of sophisticated statistical tests are available to test the reliability and validity of the proposed regression models and specific regression relationships in more detail, to investigate their specific properties and to detect even their less obvious shortcomings. These may be, for example, normality tests, autocorrelation tests, and homoskedasticity tests, the procedural principles of which are elaborated, e.g., in [19].

### 9.3. Evaluation of the Differences between the Obtained and Imported Stress Concentration Factors

The evaluation of the differences  $\Delta\alpha_{Ct}$  and  $\Delta\alpha_{Ti}$  between the stress concentration factors  $\alpha_{VM}$  obtained by FEM analyses and the imported stress concentration factors  $\alpha_{Ct}$  and  $\alpha_{Ti}$  is performed in two bands separately for  $D/d$  in the 1st band from 1.01 to 1.10 and in the 2nd band from 1.2 to 3.0.

In the 1st  $D/d$  band from 1.01 to 1.10, the lines for  $\Delta\alpha_{Ct}$  form a relatively compact bundle of lines in a relatively narrow range of approximately  $-3$ – $0\%$ . The only exception is the line for the largest ratio  $D/d = 1.10$ , for which in the lower  $r/d$  range the of  $\Delta\alpha_{Ct}$  value reaches an anomalous level of up to  $-8\%$ . This implies that the  $\alpha_{Ct}$  quantities are slightly to moderately underestimated in this  $D/d$  band relative to the  $\alpha_{VM}$  quantities. The lines for  $\Delta\alpha_{Ti}$  are already less compact with respect to each other. There is a tendency for  $\alpha_{Ti}$  to be significantly underestimated relative to  $\alpha_{VM}$  in the range  $-13$  to  $-7\%$  for  $D/d = 1.01$  to a tendency for  $\alpha_{Ti}$  to be slightly overestimated relative to  $\alpha_{VM}$  in the range  $7.5$ – $5\%$  for  $D/d = 1.10$ . Thus, overall, the values of  $\alpha_{Ct}$  and  $\alpha_{Ti}$  relative to the values of  $\alpha_{VM}$  in this  $D/d$  band range with a difference in the larger interval  $-13$  to  $7.5\%$  for the lower  $r/d$  range to the gradually narrowing interval  $-7$  to  $5\%$  for the upper  $r/d$  range.

In the 2nd band, i.e., for  $D/d$  from 1.2 to 3.0 in terms of the differences  $\Delta\alpha_{Ct}$  and  $\Delta\alpha_{Ti}$ , a remarkable phenomenon can be observed to some extent. Indeed, in the compactness/non-compactness and underestimation/overestimation tendencies, the quantities  $\alpha_{Ct}$  and  $\alpha_{Ti}$  have switched roles. The quantities  $\Delta\alpha_{Ct}$  form a less compact bundle of lines. At the same time, there is a tendency for the  $\alpha_{Ct}$  quantity to underestimate the  $\alpha_{VM}$  quantity in the range  $-7$  to  $-3\%$  for the lower range of  $r/d$  values and all  $D/d$  ratios to a tendency for the

$\alpha_{Ct}$  quantity to overestimate the  $\alpha_{VM}$  quantity in the range 0–6% for the upper range of  $r/d$  values and again for all  $D/d$  ratios. The  $\Delta\alpha_{Ti}$  quantities here form a fairly compact bundle of lines in the range 6.5–9% for the lower range of  $r/d$  values and all  $D/d$  ratios to the range 5–7% for the upper range of  $r/d$  values and all  $D/d$  ratios. Hence, the  $\alpha_{Ti}$  quantities are overestimated in this  $D/d$  range relative to the  $\alpha_{VM}$  quantities in the range of 5–9% for the entire range of  $r/d$  ratios. Thus, overall, the values of  $\alpha_{Ct}$  and  $\alpha_{Ti}$  relative to the values of  $\alpha_{VM}$  in this  $D/d$  band range with a difference in the larger interval of 7 to 9% for the lower  $r/d$  range to a progressively narrower interval of 0 to 7% for the upper  $r/d$  range.

The tendency for the range of differences of the values of the stress concentration factors  $\alpha_{Ct}$  and  $\alpha_{Ti}$  to change with respect to the values of  $\alpha_{VM}$  from the lower range of  $r/d$  ratios (the larger range of differences  $\Delta\alpha$ ) to the upper range of  $r/d$  ratios (the smaller range of differences  $\Delta\alpha$ ) is exactly the same in the two bands for  $D/d$ .

Thus, in some cases, the analyses found differences dependent on the  $r/d$  ratio with no apparent dependence on  $D/d$ . In some other cases, the opposite was true. In the remaining cases, no trend dependence was found, i.e., neither on  $r/d$  ratios nor on  $D/d$  ratios.

Similar conclusions about the ambiguity of the results can be found in the relevant literature. For example, according to several data from available sources, some authors, based on experimental measurements with the Photostress<sup>®</sup> method, consider the waveforms or their analytical dependencies according to [15] or from the corresponding older versions to be correct, or for some  $d/D$  ratios to be slightly overestimated. According to [20], similar conclusions can be drawn on the basis of FEM analyses. On the contrary, according to other FEM analyses performed, e.g., by Tipton et al. [18], these results are underestimated, with a difference of up to 40% being reported in some cases. More details are given in Section 5, where Tipton recommends to use formula (12).

## 10. Possible Reasons for Differences between the Analyzed and Compared Data

Explaining the reasons for the differences in the data obtained is a good topic for further analysis and research. The source of these differences may be determined by a number of factors. To achieve the relevant criteria of reliability and validity, the methodology for the preparation and implementation of the modelling (analytical, experimental, numerical, combined) and the subsequent evaluation and interpretation of the results will play an important role. For example, if the emphasis is on the accurate determination of the values of the stress concentration factors, it is not appropriate to start from an approximation equation for geometric parameter configurations for which there is no corresponding curve or dependence in the graphs and diagrams. This may also be the case if the value sought is the limiting, i.e., initial or final, value of the curve, or there is a reading outside the specified range. Deviations from reality may also be cumulated, for example, by inaccuracy of the data due to inaccurate readings from graphical sources of information, e.g., diagrams and nomograms. The lack of accuracy of any approximation equation may also be a source of problems. In the case of experimental solutions, typically, e.g., by the Photostress<sup>®</sup> method, it is a question of the quality of the experimental object, i.e., the physical model, namely its geometric and dimensional accuracy, the quality of the optically sensitive material, the methods of fitting and loading the model, etc. In the case of an experiment, it is also a question of the reliability achieved, the accuracy and sensitivity of the measurement chain used, the correctness of the data reading location, particularly the extremes, the choice of suitable sensors, etc. In the case of numerical solutions, typically, e.g., by applying FEM, it is a question of the choice of the appropriate software, the type of analysis, the development of the numerical model, the type of finite elements applied, the quality and quantity of meshing, the choice of boundary conditions, etc.

At the same time, other more complex factors that may influence or distort the results are not mentioned in this evaluation. These include, for example, the issue or consideration of the occurrence of microplastic deformation, linking the analyses to factors related to fracture mechanics issues, etc. In addition, the subject of the analysis was a simple configu-

ration in which, for example, the optimization of the shape and dimensions of the transition curve was not addressed.

## 11. Conclusions

The study presented in this paper, on the basis of the analyses performed and the comparison of the corresponding results, points to the fact that even for such configurationally relatively simple cases of shape-discontinuity-dimensions-load design elements, there is no or cannot be a generally unambiguous recommendation of a preferred approach to the choice of data or information source or to the method of obtaining it. From the analyses and simulations carried out, it is difficult to conclude clearly which of the methods compared for determining the stress concentration factors underestimates or overestimates the notching effect of a sudden change in shaft cross-section by a certain margin. At the same time, therefore, it is not possible to determine unambiguously and objectively the accuracy of any particular approach or data source. It is only possible to state positive or negative differences or a tendency to relative underestimation or overestimation without determining the degree of correctness of the solution. Moreover, it is not possible to put these differences into a clear and obvious connection or continuity with respect to either the origin of the data source or modelling (analytical, experimental, numerical, combined) or with respect to the values of the input parameters, e.g., the ratios  $r/d$  and  $D/d$  as independent variables.

The above issues are also fully applicable to the continuously emerging new cases of stress concentrators, which have not yet been analyzed at all from the point of view of stress concentration factors. Until such a time when appropriate methodologies have been developed and verified in practice, it is of course possible to continue to make use of existing available data and data sources. It is just necessary to be constantly aware of and take into account the relevant or certain degree of uncertainty. Thus, it is precisely the knowledge of which approach, and to what extent, underestimates or overestimates the relevant notching effect more that can be welcome information for the designer in this process. Another piece of information provided by this paper is the regression analysis of some of the data obtained by FEM analysis in the form of individual regression dependencies.

**Author Contributions:** P.S., conceptualization, project administration, supervision, and writing; I.D., draft preparation, computation, and visualization; J.B., methodology and validation. All authors have read and agreed to the published version of the manuscript.

**Funding:** This work was supported by the Slovak Research and Development Agency under the grant project VEGA No. 1/0500/20.

**Institutional Review Board Statement:** Not applicable.

**Informed Consent Statement:** Not applicable.

**Data Availability Statement:** The data presented in this study are available on request from the corresponding author. The data are not publicly available due to the large amount.

**Conflicts of Interest:** The authors declare no conflict of interest.

## References

1. Wei, L.; Zhaoyang, M.; Longkang, L.; Zhongwen, Y. Photoelastic evaluation of stress fields and notch stress intensity factors for blunt V-notches. *Theor. Appl. Fract. Mech.* **2020**, *110*, 102806. [[CrossRef](#)]
2. Santos, A.; Guzman, R.; Ramirez, Z.; Cardenas, C. Simulation of stress concentration factors in combined discontinuities on flat plates. *J. Phys. Conf. Ser.* **2016**, *743*, 012014. [[CrossRef](#)]
3. Kántor, D. Determination of Stress Concentration Factors by Numerical Analysis and Their Comparison with Experimentally Obtained Values. Master's Thesis, Technical University of Košice, Košice, Slovak, 2022. (In Slovak/Czech).
4. Pedersen, N.L. Aspects of stress in optimal shaft shoulder fillet. *J. Strain Anal. Eng. Des.* **2018**, *53*, 285–294. [[CrossRef](#)]
5. Menčík, J. *Applied Mechanics of Materials*; Polygraphic Centre of the University of Pardubice: Pardubice, Czech Republic, 2019; p. 196, (Original In Czech).
6. Taylor, D.; Kelly, A.; Toso, M.; Susmel, L. The variable-radius notch: Two new methods for reducing stress concentration. *Eng. Fail. Anal.* **2011**, *18*, 1009–1017. [[CrossRef](#)]

7. Kunz, J. *Applied Fracture Mechanics*, 1st ed.; Czech Technology—Czech Technical University Publishing House: Prague, Czech Republic, 2005; p. 273, (Original In Czech).
8. Delyová, I.; Hroncová, D.; Sivák, P. Use of FEM in identification of stress in place of concentration factor. *Am. J. Mech. Eng.* **2016**, *4*, 454–459.
9. Trebuňa, F.; Šimčák, F. *Resistance of Elements of Mechanical Systems*; Emilena: Košice, Slovak, 2004; (Original In Slovak).
10. Makhutov, N.A.; Reznikov, D.O. Generalization of Neuber's rule for the assessment of local stresses and strains in stress concentration zones for a wide range of applied strains. *Procedia Struct. Integr.* **2019**, *14*, 199–206. [[CrossRef](#)]
11. Chmelko, V. *Notching Effects in the Operation of Machines and Structures*; Slovak University of Technology: Bratislava, Slovak, 2015; p. 136. ISBN 978-80-227-4482-9. (Original In Slovak).
12. Mumovic, A.J.; Saric, I.; Repcic, N. Numerical analysis of stress concentration factors. *Procedia Eng.* **2015**, *100*, 707–713. [[CrossRef](#)]
13. Hearn, J. *Mechanics of Materials 2: The Mechanics of Elastic and Plastic Deformation of Solids and Structural Materials*, 3rd ed.; Elsevier: Amsterdam, The Netherlands, 1997; p. 539.
14. Shigley, J.E.; Mischke, C.R.; Budynas, R.G. *Mechanical Engineering Design*; Chapter 7; McGrawHill: New York, NY, USA, 2001.
15. Pilkey, W.D.; Bi, Z.; Pilkey, D.F. *Peterson's Stress Concentration Factors*, 4th ed.; John Wiley & Sons: Hoboken, NJ, USA, 2020.
16. Sonmez, F. Optimal shape design of shoulder fillets for flat and round bars under various loadings. *J. Mech. Eng. Sci.* **2009**, *223*, 1741–1754. [[CrossRef](#)]
17. Norton, R.L. *Machine Design—An Integrated Approach*, 4th ed.; Worcester Polytechnic Institute, Pearson: London, UK, 2010; p. 1056. ISBN 978-0-13-612370-5.
18. Tipton, S.M.; Sorem, J.R.; Rolovic, R.D. Updated stress concentration factors for filleted shafts in bending and tension. *J. Mech. Des.* **1996**, *118*, 321. [[CrossRef](#)]
19. Frankovský, P.; Sivák, P.; Delyová, I.; Hroncová, D.; Štuller, P. Rectification of gas pipeline bridging with the support of experimental stress analysis and means of regression and correlation analysis. *Appl. Sci.* **2022**, *12*, 10555. [[CrossRef](#)]
20. ESDU. *Stress Concentrations, Engineering Science*; Data Unit: London, UK, 1989.

**Disclaimer/Publisher's Note:** The statements, opinions and data contained in all publications are solely those of the individual author(s) and contributor(s) and not of MDPI and/or the editor(s). MDPI and/or the editor(s) disclaim responsibility for any injury to people or property resulting from any ideas, methods, instructions or products referred to in the content.